Adaptive optics with advanced phase-contrast techniques. II. High-resolution wave-front control

Eric W. Justh

Institute for Systems Research, University of Maryland, College Park, Maryland 20742

Mikhail A. Vorontsov

Intelligent Optics Laboratory, U.S. Army Research Laboratory, Adelphi, Maryland 20783

Gary W. Carhart

Intelligent Optics Laboratory, U.S. Army Research Laboratory, Adelphi, Maryland 20783

Leonid A. Beresnev

Intelligent Optics Laboratory, U.S. Army Research Laboratory, Adelphi, Maryland 20783

P. S. Krishnaprasad

Department of Electrical and Computer Engineering and Institute for Systems Research, University of Maryland, College Park, Maryland 20742

Received April 7, 2000; revised manuscript received November 17, 2000; accepted November 17, 2000

A wave-front control paradigm based on gradient-flow optimization is analyzed. In adaptive systems with gradient-flow dynamics, the output of the wave-front sensor is used to directly control high-resolution wave-front correctors without the need for wave-front phase reconstruction (direct-control systems). Here, adaptive direct-control systems with advanced phase-contrast wave-front sensors are analyzed theoretically, through numerical simulations, and experimentally. Adaptive system performance is studied for atmospheric-turbulence-induced phase distortions in the presence of input field intensity scintillations. The results demonstrate the effectiveness of this approach for high-resolution adaptive optics. © 2001 Optical Society of America

OCIS codes: 010.1080, 010.7350, 070.2580, 070.4340, 120.5050.

1. INTRODUCTION

In Part I of this study[1] we analyzed high-resolution wave-front sensors based on the classical phase-contrast technique (Zernike filter and point-diffraction interferometer). The major advantage of these sensors for adaptive optics applications lies in the possibility of using sensor output to control the wave-front shaping device directly, without the extensive computations required for mapping sensor data to deformable-mirror control signals through conventional phase or control matrix reconstruction techniques. Here we analyze these new direct-control adaptive optics architectures through theoretical study, numerical analysis, and proof-of-concept experiments. The direct-control adaptive optics architecture described here has a potential for transitioning to high-resolution adaptive systems that contain a large number ($N \approx 10^3-10^5$) of control channels.

In Section 2 we introduce a theoretical basis for direct-control adaptive optics. The wave-front control algorithm is considered here as a continuous-time gradient-flow procedure for maximization of the adaptive system performance metric J (cost functional), dependent on both the controlling phase $u(\mathbf{r}, t)$ introduced by the wave-front corrector and the input wave-front phase $\varphi(\mathbf{r}, t)$. It is shown that for adaptive systems that aim to maximize the Strehl ratio St (or, equivalently, the intensity of the output field's zero-order spectral component), the gradient $J'(\mathbf{r}, t)$ of the cost functional $J[u] = \mathrm{St}$ can be calculated analytically. The remarkable fact is that this gradient is proportional to the output signal $I_{\mathrm{out}}(\mathbf{r}, t)$ of the differential Zernike filter introduced in Part I of this study.[1] This result offers a practical method for both making gradient measurements and implementing direct-control adaptive optical systems by use of the gradient-flow optimization paradigm.

In Section 3 we analyze direct-control adaptive systems with conventional and optoelectronic Zernike sensors. Despite the fact that gradient-flow dynamics apply to these systems only locally (in the range of small-amplitude phase distortions), simulation results show that efficient phase-distortion compensation takes place over a wide range of phase-distortion amplitudes. A nu-

0740-3232/2001/061300-12$15.00

merical analysis of direct-control adaptive systems in the presence of atmospheric-turbulence-induced phase distortions is presented in Section 4 for both uniform and randomly modulated input wave intensity distributions. Results include an analysis of direct-control systems with the following wave-front sensors: conventional, optoelectronic, nonlinear, and differential Zernike filters. It is shown that for relatively small-intensity scintillation levels (10–15%), all of these systems are capable of achieving efficient phase-distortion compensation. However, when the intensity scintillation level is increased, the performance of most systems declines, except for the adaptive system with the differential Zernike sensor. The direct-control adaptive system with the differential Zernike filter demonstrates exceptionally high performance in phase-distortion compensation, even in the presence of strong intensity scintillations. Results of the proof-of-concept experiments with an adaptive system that has a 127-element liquid-crystal (LC) phase modulator and a nonlinear Zernike filter with an optically controlled LC light-valve phase modulator are presented in Section 5.

2. WAVE-FRONT CONTROL BASED ON GRADIENT-FLOW OPTIMIZATION

A. Feedback-Controller Synthesis

Consider the direct-control adaptive optics system shown in Fig. 1. This system consists of the following adaptive optics components: wave-front corrector, wave-front sensor, and feedback controller. All of the adaptive system components are assumed to have high spatial resolution, and thus a continuously distributed approximation of the adaptive system model can be used. The wave-front corrector introduces a phase modulation $u(\mathbf{r}, t)$ into the distorted input wave $A_{\text{in}}(\mathbf{r}, t) = A_0(\mathbf{r})\exp[i\varphi(\mathbf{r}, t)]$. The corrected wave $A_{\text{cor}}(\mathbf{r}, t) = A_0(\mathbf{r})\exp\{i[\varphi(\mathbf{r}, t) + u(\mathbf{r}, t)]\}$ is used as the wave-front sensor input. The wave-front sensor is interfaced with the feedback controller, which operates directly by using the sensor's output intensity $I_{\text{out}}(\mathbf{r}, t)$.

The dependence of the correction function u on the wave-front sensor output I_{out} defines the control algorithm built into the feedback controller. For a continuous-time controller this algorithm can be represented as a time-dependent controlling phase-evolution process:

$$\frac{\partial u(\mathbf{r}, t)}{\partial t} = G(u, I_{\text{out}}), \tag{1}$$

where G is an operator describing the feedback controller.

Synthesis of the wave-front controller G can be based on different principles. In the diffractive-feedback adaptive system, both the wave-front sensor and the controller G are selected on the basis of an analysis of the nonlinear spatiotemporal dynamics of expression (1).[2,3] The major requirement for these dynamics, or equivalently for the feedback controller design, is the existence of stationary-state solutions [expression (1)] that correspond to phase-distortion suppression.

Another approach to wave-front controller synthesis is based on the gradient optimization technique.[4–6] In this case the control rule (1) describes a continuous-time gradient-descent optimization of a system performance metric J:

$$\frac{\partial u(\mathbf{r}, t)}{\partial t} = \eta J'(\mathbf{r}, t), \tag{2}$$

where $J'(\mathbf{r}, t)$ is a first variation (gradient) of the cost functional and η is a constant positive for cost functional maximization and negative otherwise. There are two approaches that can be used for practical implementation of the gradient-descent algorithm [expression (2)]: model-free and gradient-flow optimization. In the model-free optimization technique, an approximation $\tilde{J}'(\mathbf{r}, t)$ is used instead of the "true" gradient $J'(\mathbf{r}, t)$. This approximation can be obtained by applying a small perturbation δu to the wave-front corrector and measuring the corresponding change δJ of the system performance metric. For the recently developed parallel stochastic gradient-descent technique, the gradient approximation used is proportional to the product $\delta J\, \delta u$.[7–10] The relatively low convergence rate is the major drawback of the model-free optimization technique, particularly noticeable for high-resolution adaptive optics.

A different idea is utilized in the gradient-flow optimization method, which is widely used for digital image-processing applications.[11–13] The gradient $J'(\mathbf{r}, t)$ is calculated analytically based on knowledge of the system's mathematical model and performance metric. The problem is that in most adaptive optics applications, the system model, which includes phase aberrations, is unknown. In addition, for practical implementation of the gradient-flow technique in adaptive optics, the gradient $J'(\mathbf{r}, t)$ should be dependent only on available information: Here, the wave-front sensor output intensity $I_{\text{out}}(\mathbf{r}, t)$ and the controlling phase $u(\mathbf{r}, t)$. This requires gradient representation in the following form: $J'(\mathbf{r}, t) = J'[u, I_{\text{out}}]$. As is shown in the following sections, the gradient-flow direct-control technique can indeed be used for adaptive wave-front distortion correction.

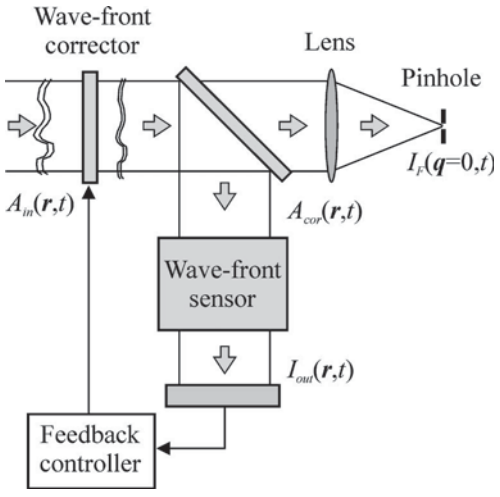

Fig. 1. Schematic of a direct-control adaptive optics system.

B. System Performance Metric and Gradient-Flow Dynamics

For a number of adaptive optics applications (e.g., imaging of point-source objects, laser communication), a natural measure of system performance in correcting the aberrated wave front is the Strehl ratio $\mathrm{St} = I_F(\mathbf{q} = 0)/I_F^0$. Here $I_F(\mathbf{q})$ is the intensity of the output wave in the lens's focal plane (Fig. 1) and I_F^0 is the corresponding intensity in the absence of phase aberrations. Maximization of the Strehl ratio by the gradient-descent technique may result in two undesirable phenomena: drift of the aperture-averaged phase $\bar{u}(t)$ toward the edge of the wave-front corrector's operational range, and phase discontinuities, both of which may occur during the adaptation process. To prevent aperture-averaged phase drift and to smooth the controlling phase (i.e., to suppress discontinuities and noise) the system performance metric J may include (besides the Strehl ratio) additional penalty terms:

$$J[u] = \mathrm{St} - \alpha_1[\bar{u}(t) - u_0]^2 - \alpha_2 \int |\nabla u(\mathbf{r}, t)|^2 \mathrm{d}^2\mathbf{r}, \tag{3}$$

where $\bar{u}(t) = S^{-1}\int u(\mathbf{r}, t)\mathrm{d}^2\mathbf{r}$ is the phase averaged over the aperture area S, u_0 is a desirable value for $\bar{u}(t)$, and α_1 and α_2 are weight coefficients determining penalty term contributions. For now, ignore in Eq. (3) the time dependence of both phase aberrations and the controlling phase by assuming that phase aberrations are stationary state ("frozen"). The complex amplitude of the input field (after it passes through the wave-front corrector) can then be represented in the form $A_{\mathrm{cor}}(\mathbf{r}) = A_0(\mathbf{r})\exp\{i[u(\mathbf{r}) + \tilde{\phi}(\mathbf{r})]\}$. Using the notation introduced in Part 1,[1] instead of expression (3) we obtain

$$\begin{aligned} J[u] = &\left| \int A_0(\mathbf{r})\exp\{i[u(\mathbf{r}) + \tilde{\varphi}(\mathbf{r})]\}\mathrm{d}^2\mathbf{r} \right|^2 \\ &- \beta_1\left[u_0 - S^{-1}\int u(\mathbf{r})\mathrm{d}^2\mathbf{r}\right]^2 \\ &- \beta_2 \int |\nabla u(\mathbf{r})|^2 \mathrm{d}^2\mathbf{r}, \end{aligned} \tag{4}$$

where $\tilde{\varphi}(\mathbf{r}) = \varphi(\mathbf{r}) - \bar{\varphi}$ is the spatially modulated component of the wave-front aberration and β_1 and β_2 are new weight coefficients. The first term in expression (4) is proportional to the intensity of the input field's zero-order spectral component $I_F(\mathbf{q} = 0)$. Note that expressions for the weighting coefficients in expression (4) are irrelevant for the analysis below and for this reason are not defined. Consider the variation δJ of the cost functional resulting from the small perturbation δu of the controlling phase:

$$\delta J = J[u + \delta u] - J[u] = \int J'(\mathbf{r})\delta u(\mathbf{r})\mathrm{d}^2\mathbf{r} + o(\delta u), \tag{5}$$

where the term $o(\delta u)$ describes second- and higher-order terms with respect to the phase variation δu. Using expression (5) for the cost functional gradient we obtain (see Appendix A)

$$\begin{aligned} J' = &-2|\bar{A}_0|A_0(\mathbf{r})\sin[u(\mathbf{r}) + \tilde{\varphi}(\mathbf{r}) - \Delta] - 2\beta_1(\bar{u} - u_0) \\ &+ 2\beta_2\nabla^2 u(\mathbf{r}). \end{aligned} \tag{6}$$

Here

$$\bar{A}_0 \equiv |\bar{A}_0|\exp(i\Delta) = \int A_0(\mathbf{r})\exp\{i[u(\mathbf{r}) + \tilde{\varphi}(\mathbf{r})]\}\mathrm{d}^2\mathbf{r}.$$

Note that the value $|\bar{A}_0|^2$ in Eq. (6) is proportional to the Strehl ratio.

Embed the control function $u(\mathbf{r})$ in a family of time-dependent functions $u(\mathbf{r}, t)$, and consider the time-dependent evolution of J in the direction of the cost functional gradient. Thus the gradient-flow dynamics (2) leads to the following nonlinear diffusion equation describing the controlling phase update:

$$\begin{aligned} \frac{\partial u(\mathbf{r}, t)}{\partial t} = &\, d\nabla^2 u(\mathbf{r}, t) \\ &- \gamma|\bar{A}_0(t)|A_0(\mathbf{r})\sin[u(\mathbf{r}, t) + \tilde{\varphi}(\mathbf{r}) - \Delta] \\ &- \mu[\bar{u}(t) - u_0], \end{aligned} \tag{7}$$

where d, γ, and μ are coefficients dependent on the parameters α_1, α_2, and η introduced in expressions (2) and (3).

C. Gradient-Flow Dynamics and Adaptive-Feedback-Controller Synthesis

Compare the sinusoidal term in the formula for the gradient [Eq. (6)] with the expression for the output intensity for the differential Zernike wave-front sensor described in Part I[1]:

$$\begin{aligned} I_{\mathrm{dif}}(\mathbf{r}, t) &\equiv \tfrac{1}{2}\left[I_{\mathrm{zer}}^{(+)}(\mathbf{r}, t) - I_{\mathrm{zer}}^{(-)}(\mathbf{r}, t)\right] \\ &= 2A_0(\mathbf{r})|\bar{A}_0(t)|\sin[u(\mathbf{r}, t) + \tilde{\varphi}(\mathbf{r}) - \Delta], \end{aligned} \tag{8}$$

where $I_{\mathrm{zer}}^{(+)}(\mathbf{r}, t)$ and $I_{\mathrm{zer}}^{(-)}(\mathbf{r}, t)$ are the differential Zernike wave-front sensor output intensity distributions corresponding to phase shifts $\pi/2$ and $-\pi/2$, respectively, of the field zero-order spectral component.

The key observation from this comparison is that the gradient (6) can be represented in a form dependent only on the wave-front sensor output intensity $I_{\mathrm{dif}}(\mathbf{r}, t)$ and controlling phase $u(\mathbf{r}, t)$, that is, in the form $J'(\mathbf{r}, t) = J'[u, I_{\mathrm{dif}}]$ required for adaptive system feedback-controller synthesis:

$$J' = -I_{\mathrm{dif}}(\mathbf{r}, t) - 2\beta_1(\bar{u} - u_0) + 2\beta_2\nabla^2 u(\mathbf{r}, t). \tag{9}$$

Correspondingly, Eq. (7) for the feedback controller based on the differential Zernike filter reads

$$\frac{\partial u(\mathbf{r}, t)}{\partial t} = d\nabla^2 u(\mathbf{r}, t) - KI_{\mathrm{dif}}(\mathbf{r}, t) - \mu[\bar{u}(t) - u_0], \tag{10}$$

where the coefficient K is proportional to γ in Eq. (7). The most important conclusion from this analysis is the following: The feedback controller (10) is an implementation of continuous-time gradient-flow dynamics, leading to a maximization of the cost functional (4). It can be shown that during the adaptation process, the time derivative of J is always positive ($\mathrm{d}J/\mathrm{d}t > 0$); that is, the

feedback controller (10) provides for a monotonic increase in Strehl ratio. Note that Eq. (10) was obtained for an input wave that has an arbitrary (nonuniform) intensity distribution, $I_0(\mathbf{r}) = A_0^2(\mathbf{r})$. This suggests an essential characteristic of the gradient-flow feedback controller (10): Maximization of the Strehl ratio should occur even in the presence of input wave intensity modulation.

The discrete-time version of Eq. (10) corresponds to the following iterative wave-front correction algorithm:

$$u^{(n+1)}(\mathbf{r}) = u^{(n)}(\mathbf{r}) + d\nabla^2 u^{(n)}(\mathbf{r}) - KI_{\mathrm{dif}}^{(n)}(\mathbf{r}) - \mu[\bar{u}^{(n)} - u_0], \tag{11}$$

where the index n defines the iteration number. This algorithm describes the adaptive system's closed-loop controller. For a pixelated (piston-type) high-resolution wave-front corrector (LC or micromechanical mirror array), the control algorithm [expression (11)] reads as

$$u^{(n+1)}(\mathbf{r}_{i,j}) = u^{(n)}(\mathbf{r}_{i,j}) + d\nabla^2 u^{(n)}(\mathbf{r}_{i,j}) - KI_{\mathrm{dif}}^{(n)}(\mathbf{r}_{i,j}) - \mu[\bar{u}^{(n)} - u_0], \tag{12}$$

where $u^{(n)}(\mathbf{r}_{i,j})$ is the phase shift of an individual wave-front corrector element (pixel) with coordinate $\mathbf{r}_{ij}$ at the nth iteration and $I_{\mathrm{dif}}^{(n)}(\mathbf{r}_{i,j})$ is the output signal of the corresponding pixel from the differential Zernike filter photo array. We assume that both the pixelated wave-front corrector and the Zernike filter photo array are matched in the sense that they have the same number of pixels and pixel geometry. The operator $\nabla^2 u^{(n)}(\mathbf{r}_{i,j})$ describes a local diffusive-type interaction between neighboring pixels. The algorithm (12) requires relatively simple computations that can be performed in parallel on analog very-large-scale-integration (VLSI) microelectronic systems.[14,15] The diffusion term in Eq. (11) can be excluded if smoothness of the wave-front phase modulation $u(\mathbf{r})$ is not required. In this case the adaptive-feedback-control algorithm has the simpler form

$$u^{(n+1)}(\mathbf{r}_{i,j}) = u^{(n)}(\mathbf{r}_{i,j}) + KI_{\mathrm{dif}}^{(n)}(\mathbf{r}_{i,j}) - \mu[\bar{u}^{(n)} - u_0]. \tag{13}$$

In accordance with Eq. (13) the output signals from a differential Zernike filter photo array (after scaling by the factor K and dc component subtraction) are directly (point-to-point) mapped to the wave-front corrector array signals. This controller can be integrated with the differential Zernike filter imaging sensor, providing feedback control computation directly on the imager chip.

3. DIRECT-CONTROL ADAPTIVE SYSTEMS WITH PHASE-CONTRAST SENSORS

A. Wave-Front Control with Zernike Sensors: Analysis

The major drawback of the differential Zernike wave-front sensor is the time delay associated with the measurement and subtraction of the two intensity distributions $I_{\mathrm{zer}}^{(+)}(\mathbf{r}, t)$ and $I_{\mathrm{zer}}^{(-)}(\mathbf{r}, t)$, corresponding to $\pi/2$ and $-\pi/2$ phase shifts, respectively. In contrast, as described in Part I,[1] conventional, optoelectronic, and nonlinear Zernike wave-front sensors require only a single intensity-distribution measurement. A natural question to ask is whether the gradient-flow dynamics of the differential Zernike filter feedback system carry over to the corresponding adaptive optical system based on the use of conventional phase-contrast techniques. Recall from Part I that the output intensity distribution for the conventional Zernike filter is given by

$$I_{\mathrm{out}}(\mathbf{r}, t) = I_0(\mathbf{r}) + 2|\bar{A}_0(t)|^2 - 2A_0(\mathbf{r}) \times |\bar{A}_0(t)|\{\cos[u(\mathbf{r}, t) + \tilde{\varphi}(\mathbf{r}) - \Delta] - \sin[u(\mathbf{r}, t) + \tilde{\varphi}(\mathbf{r}) - \Delta]\}. \tag{14}$$

Besides the sine term present in the differential Zernike filter output (8), expression (14) contains three additional terms. With use of (8), Eq. (14) can be represented in the following form:

$$I_{\mathrm{out}}(\mathbf{r}, t) = I_{\mathrm{dif}}(\mathbf{r}, t) + I_0(\mathbf{r}) + 2|\bar{A}_0(t)|^2 - 2A_0(\mathbf{r})|\bar{A}_0(t)|\cos[u(\mathbf{r}, t) + \tilde{\varphi}(\mathbf{r}) - \Delta]. \tag{15}$$

Similarly to Eq. (10), a feedback controller based on the use of the conventional Zernike filter can be represented in the form

$$\frac{\partial u(\mathbf{r}, t)}{\partial t} = d\nabla^2 u(\mathbf{r}, t) - KI_{\mathrm{out}}(\mathbf{r}, t) - \mu[\bar{u}(t) - u_0]. \tag{16}$$

Note that the dynamical process (16) no longer describes gradient-flow dynamics. Indeed, by using expressions (9) and (15) instead of expression (16) we obtain

$$\frac{\partial u(\mathbf{r}, t)}{\partial t} = \eta J'(\mathbf{r}, t) - \kappa_1 I_0(\mathbf{r}) - \kappa_2|\bar{A}_0(t)|^2 + \kappa_3 A_0(\mathbf{r})|\bar{A}_0(t)|\cos[u(\mathbf{r}, t) + \tilde{\varphi}(\mathbf{r}) - \Delta], \tag{17}$$

where κ_1, κ_2, and κ_3 are weighting coefficients. The right-hand side of Eq. (17) contains additional terms that may potentially destroy the gradient-flow dynamics. To evaluate the influence of these "parasitic" terms, we simplify the problem by assuming that the input beam intensity distribution is uniform, i.e., that $I_0(\mathbf{r}) = I_0 = \text{constant}$. In this case the term $\kappa_1 I_0 + \kappa_2|\bar{A}_0|$ on the right-hand side of Eq. (17) is spatially uniform and introduces an additional constant phase shift that has no effect on the dynamics. Indeed, this additional phase shift is automatically compensated by the penalty term in the cost-functional (4) that prevents the average phase from drifting away from some specified value u_0. A more complicated issue is the effect of the cosine term in Eq. (17). Assume that the residual (uncompensated) phase distortion $w(\mathbf{r}, t) = u(\mathbf{r}, t) + \tilde{\varphi}(\mathbf{r})$ is small ($|w| \ll 1$ for all $\mathbf{r}$) and hence the value Δ in Eq. (17) approaches zero. In the linear approximation the cosine term in Eq. (17) approaches the constant $\kappa_3 A_0|\bar{A}_0|\cos[u(\mathbf{r}, t) + \tilde{\varphi}(\mathbf{r}) - \Delta] \approx \kappa_3 A_0|\bar{A}_0|$, which does not affect system dynamics. Therefore, for relatively small-amplitude phase distortions, dynamics of the adaptive system with the conventional Zernike filter (16) are governed by the same gradient term as the dynamics of the system based on the differential Zernike wave-front sensor (10).

As a result, the global gradient-flow behavior of the differential Zernike filter feedback system applies to the adaptive feedback system with a conventional Zernike filter only locally, in the vicinity of small-amplitude phase aberrations. The simulation results described below suggest, however, that the convergence behavior of the Zernike filter feedback system may actually be fairly robust and can be extended beyond the range of small-amplitude phase distortions.

This result can be explained if we consider stationary-state solutions of Eq. (17) for uniform input beam intensity and in the absence of the diffusion term ($d = 0$). These solutions (if they exist) satisfy the following equation obtained from Eq. (17) for $t \to \infty$:

$$-Kc_1\{\cos[u(\mathbf{r}) + \tilde{\varphi}(\mathbf{r}) - \Delta] - \sin[u(\mathbf{r}) + \tilde{\varphi}(\mathbf{r}) - \Delta]\} + c_2 = 0,$$

where c_1 and c_2 are constant values. For a sufficiently large feedback coefficient ($|K| > |c_2/c_1|$), stationary-state solutions can be represented in the form $u(\mathbf{r}) = -\tilde{\varphi}(\mathbf{r}) + \text{constant} + 2\pi n(\mathbf{r})$, where n is an integer. The stepwise function $n(\mathbf{r})$ is dependent on both the initial conditions $u(\mathbf{r}, t = 0)$ and the phase distortions $\tilde{\varphi}(\mathbf{r})$ and can vary across the input wave cross section. Thus, control dynamics of the adaptive system with the Zernike filter may result in convergence to a number of degenerate 2π-phase-cut type solutions corresponding to the same (optimal) value of the Strehl ratio St.

The presence of the diffusion term eliminates degeneracy related to the 2π phase cuts. In this case sharp changes in the phase function are penalized by the diffusion term, resulting in a "smooth" stationary-state solution of the form $u(\mathbf{r}) = -\tilde{\varphi}(\mathbf{r}) + \text{constant} + 2\pi n$, where n has the same value for all $\mathbf{r}$. Diffusion transforms the phase-cut-related cost functional local minima into saddle-type points. The presence of saddle-type points may result in a substantial decrease in adaptation process convergence rate (Section 4).

Analysis of the system dynamics is not complete unless we examine the stability of the obtained stationary-state solutions. Consider as an example an adaptive direct-control system with a point-diffraction interferometer. Following the same procedure as is used for synthesis of the feedback controller with a Zernike filter, assume that in Eq. (16) describing the wave-front controller, $I_{\text{out}}(\mathbf{r}, t)$ represents the output pattern of the point-diffraction interferometer. From Part I[1] for uniform input field intensity we have $I_{\text{out}}(\mathbf{r}, t) \approx \cos[u(\mathbf{r}, t) + \tilde{\varphi}(\mathbf{r}) - \Delta] + \text{constant}$. Instead of the sine term present in the corresponding expressions (8) and (14) for the Zernike-filter-based wave-front sensors, this expression contains only a cosine term. In the vicinity of small-amplitude phase distortions, when Δ approaches zero, $I_{\text{out}}(\mathbf{r}, t) \approx \cos[u(\mathbf{r}, t) + \tilde{\varphi}(\mathbf{r})] + \text{constant}$. Stationary-state solutions of the corresponding Eq. (16) can be represented in the same form as the solutions obtained for the feedback controller with the Zernike filter:

$$u(\mathbf{r}) = -\tilde{\varphi}(\mathbf{r}) + \text{const.} + 2\pi n.$$

Despite this similarity it is easy to see that these stationary-state solutions are unstable, as the sensor's output is insensitive to the sign of the residual phase distortion. It can be shown that the feedback controller based on a point-diffraction interferometer is unstable and cannot be used in direct-control adaptive systems.

B. Numerical Simulation: Phase Aberration Compensation, 2π Phase Cuts, and Domain Walls

Performance of the adaptive system with both a conventional and an optoelectronic Zernike filter was analyzed numerically by use of phase distortions with the Andrews model for atmospheric-turbulence-induced phase fluctuation power spectra.[16] Simulations were performed for an input wave with a uniform intensity distribution and random phase aberration $\varphi(\mathbf{r})$ applied inside the aperture D. The strength of the input phase aberration was characterized by the standard deviation of the phase fluctuations averaged over the aperture $\sigma_\varphi = [S^{-1}\int\tilde{\varphi}^2(\mathbf{r})d^2\mathbf{r}]^{1/2}$ and by the Strehl ratio St. The numerical analysis was performed for the discrete-time version of the feedback controller (16), corresponding to the following iterative wave-front correction algorithm:

$$u^{(n+1)}(\mathbf{r}) = u^{(n)}(\mathbf{r}) + d\nabla^2 u^{(n)}(\mathbf{r}) - KI_{\text{out}}^{(n)}(\mathbf{r}) - \mu[\bar{u}^{(n)} - u_0]. \tag{18}$$

In all calculations we set $\mu = 1$ and $u_0 = 0$. The optoelectronic Zernike filter model used in the calculations corresponded to a $\pi/2$ phase shift for the spectral component $\mathbf{q}_{\max}$ that had the highest intensity level $I_F(\mathbf{q}_{\max}) \geqslant I_F(\mathbf{q})$. This system can operate in the presence of large-amplitude wave-front tilts. In the conventional Zernike filter wave-front sensor model, a phase shift of $\pi/2$ was applied to the zero spectral component $I_F(0)$. This wave-front sensor requires preliminary wave-front tilt removal. To distinguish among these adaptive system configurations, we used different notation for the Strehl ratio: St(max) for the adaptive system with an optoelectronic Zernike filter, St(0) for the conventional Zernike sensor system, and correspondingly $\text{St}_{\text{dif}}(\max)$ and $\text{St}_{\text{dif}}(0)$ for adaptive systems with differential Zernike filters based on optoelectronic and conventional sensor configurations.

For relatively small phase-distortion amplitudes ($\sigma_\varphi < 0.8$ rad), both the adaptive system with the conventional Zernike filter [St(0) system] and the system with the optoelectronic Zernike wave-front sensor [St(max) system] demonstrated efficient phase-distortion compensation. We achieved the residual phase-distortion amplitude $w = \max|w(\mathbf{r})| = \max|u(\mathbf{r}) + \tilde{\varphi}(\mathbf{r})| < 0.1$ and the corresponding Strehl ratio value $\text{St} > 0.98$ during the first 3–5 iterations by using control algorithm (18) without diffusion ($d = 0$) and during the first 10–20 iterations for the system with weak diffusion ($d = 0.005$). The adaptive-system convergence rates with both the conventional [St(0)] and the optoelectronic [St(max)] Zernike wave-front sensor were approximately the same. The convergence rate for phase aberration compensation was slightly better for the adaptive systems with the differential Zernike filter [$\text{St}_{\text{dif}}(\max)$ and $\text{St}_{\text{dif}}(0)$ systems]: One or two iterations were typically enough to achieve a Strehl ratio of $\text{St} > 0.99$.

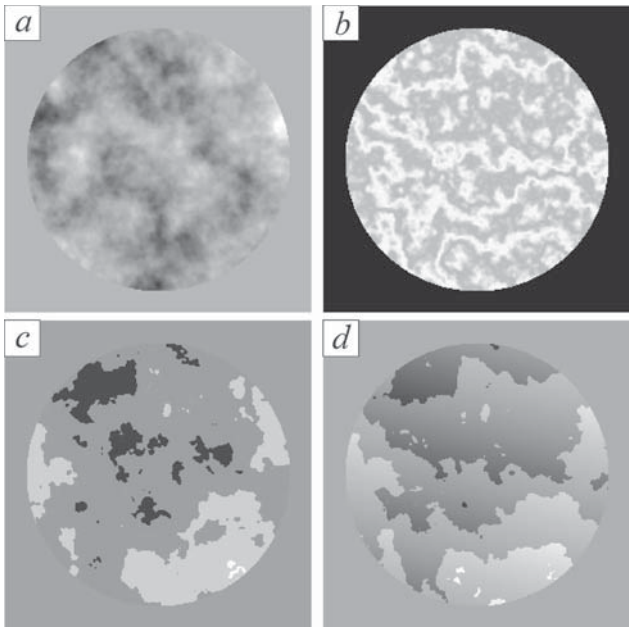

Fig. 2. Phase-distortion compensation in an adaptive system with conventional and optoelectronic Zernike filters: (a) input phase pattern, (b) output intensity distribution corresponding to (a) for a conventional Zernike filter, (c) residual phase pattern after ten iterations for the conventional and (d) residual phase pattern after ten iterations for the optoelectronic Zernike sensors. Parameters of the control algorithm are $d = 0$, $K = 0.75$, $\mu = 1$.

As mentioned in Section 3, for the case of large-amplitude ($>\pi$ rad) phase distortions the feedback controller (17) describes gradient-flow dynamics only for the system with the differential Zernike filter [$\mathrm{St}_{\mathrm{dif}}(\max)$ and $\mathrm{St}_{\mathrm{dif}}(0)$ systems]. Here we use the same notation for the Strehl ratio and for the adaptive system type. For the feedback system with conventional or optoelectronic Zernike filters [St(0) and $\mathrm{St}_{\mathrm{dif}}(\max)$ systems] the feedback controller (17) contains an unwanted cosine term that cannot be neglected. Nevertheless, for all the systems examined here we observed efficient compensation for phase distortions even when the phase-distortion amplitude increased beyond 2π rad. Increasing the aberration amplitude resulted only in a decrease of the adaptation-process convergence rate. Figure 2 shows adaptive-correction results for the phase distortion (Fig. 2a) that has a peak value amplitude near 6.5π ($\sigma_\varphi = 3.2$ rad and St = 0.011). Large-amplitude phase distortions resulted in the low-visibility output intensity pattern in Fig. 2b. The characteristic residual phase aberration patterns $w(\mathbf{r})$ corresponding to the adaptive system with conventional and optoelectronic Zernike filters are shown in Figs. 2c and Fig. 2d. In both cases the residual phase contains 2π phase cuts. These 2π phase cuts in the residual phase do not affect the performance of the idealized system with unlimited spatial resolution considered here, but they are highly undesirable in practical systems with wave-front correctors that have limited spatial resolution. Note that the adaptive system with the optoelectronic Zernike filter optimizes the intensity $I_F(\mathbf{q}_{\max})$ of the spectral component $\mathbf{q}_{\max}$ that has maximum amplitude at the beginning of the adaptation process. This causes uncompensated wave-front tilt related to the spectral component $\mathbf{q}_{\max}$ optimized by the system to be visible in the residual phase in Fig. 2d.

The 2π phase cuts in the residual phase can be removed by using control algorithm (10) or (16) with nonzero diffusion coefficient d. Indeed, in the system with diffusion, 2π phase changes can occur only within a finite distance l ($l \approx \sqrt{d}$). These sharp changes in the residual phase related to 2π phase cuts result in the appearance of narrow bright lines (domain "walls") in sensor intensity distribution $I_{\mathrm{out}}(\mathbf{r})$. These bright lines are located along boundaries separating 2π phase domains in the residual phase. It can be shown that in the system with diffusion, the 2π sharp phase changes and the corresponding domain walls in the wave-front sensor intensity are not stable. During the adaptation process the fronts of the 2π phase changes move beyond the system aperture, resulting in a "phase-cut-free" residual phase. This type of behavior of the domain walls is rather typical for dynamic systems described by nonlinear diffusion equations (Fisher–Kolmogorov–Petrovski–Piskunov-type equation.[17]) Figure 3 demonstrates the dynamics of 2π

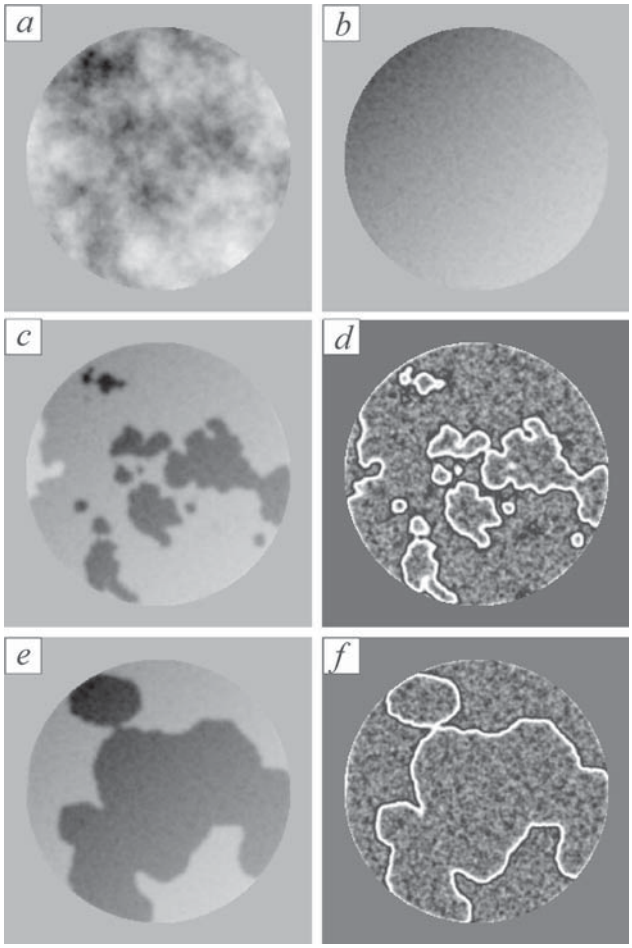

Fig. 3. Simulation results for an adaptive system with an optoelectronic Zernike filter: (a) input phase realization; (b) stationary-state residual phase pattern obtained after 100 iterations; (c), (e), residual phase and (d), (f), intensity patterns of wave-front sensor output after $N = 8$ (c and d), and $N = 32$ (e and f) iterations. System parameters are $\sigma_\varphi = 2.3$ rad (St = 0.028), $d = 0.005$, $K = 0.75$, $\mu = 1$.

phase cuts in the residual phase $w^{(n)}(\mathbf{r})$ and the corresponding dynamics of moving domain walls in wave-front sensor intensity distribution $I_{\text{out}}^{(n)}(\mathbf{r})$.

The diffusion term allows the elimination of phase cuts but leads to a significant decrease in the adaptive system's convergence speed. The phase-cut-free residual phase shown in Fig. 3b was achieved only after 100 iterations (the corresponding Strehl ratio is St = 0.95).

The phase discontinuities (2π phase cuts) observed in the direct-control system are different from phase discontinuities associated with zeros in the incident field.[18] These phase discontinuities were absent in the incident wave-front phase. The observed 2π phase cuts were formed only in the process of adaptation. The dynamical behavior of the direct-control adaptive system that has phase discontinuities in the incident field is an interesting problem that is beyond the scope of this paper.

4. STATISTICAL ANALYSIS OF ZERNIKE-FILTER-BASED ADAPTIVE SYSTEMS

A. Uniform Input Intensity

Statistical analysis of direct-control adaptive systems was performed for systems with the following wave-front sensors: conventional Zernike filter [St(0) system], optoelectronic Zernike filter [St(max) system], differential Zernike sensors with $\text{St}_{\text{dif}}(0)$ and $\text{St}_{\text{dif}}(\max)$ configurations, and nonlinear Zernike sensor (St_{nl} system). The nonlinear Zernike filter, which includes an optically controlled phase spatial light modulator (SLM) instead of the Zernike phase plate, is described in Part 1.[1]

Realizations of a statistically homogeneous and isotropic random function $\varphi(\mathbf{r})$ with zero mean and Andrews power spectrum model were used as input wave-front phase distortions (phase screens). The amplitude of the introduced phase distortions was varied by changing the value of the Fried parameter r_0.[19] For each fixed value r_0, 200 phase screens were generated. The input wave complex amplitude $A_{\text{in}}(\mathbf{r}) = A_0 \exp[i\varphi(\mathbf{r})]$ had a spatially uniform intensity of $I_0 = |A_0|^2$. A fixed number of iterations N corresponding to the discrete-time wave-front control algorithm (18) were performed for each realization of the phase-distorted input field. Adaptive system performance was evaluated by using a Strehl ratio value of St_N achieved after N iterations. For fixed Fried radius r_0 the iteration process was repeated for each of 200 phase-distortion realizations, and the obtained values St_N were averaged. The averaged Strehl ratios $\langle \text{St}_N \rangle$ are presented in Fig. 4 as functions of the ensemble-averaged standard deviation of the phase fluctuation $\sigma_{\text{in}} = \langle \sigma_\varphi \rangle$ for different iteration numbers. As expected, the adaptive system with differential optoelectronic Zernike filter [$\text{St}_{\text{dif}}(\max)$ configuration] demonstrated the most efficient phase-distortion compensation over a wide range of phase-distortion amplitudes. With this wave-front control algorithm, a Strehl ratio level of 0.98 was achieved after five iterations for $\sigma_{\text{in}} \leqslant 1.3$ rad and after ten iterations for $\sigma_{\text{in}} \leqslant 3.5$ rad. As mentioned in Section 2, the adaptive feedback-control systems based on conventional and optoelectronic Zernike sensors implement gradient-flow dynamics only locally within the vicinity of small-amplitude phase distortions ($\sigma_{\text{in}} \ll 1$). The results of the numerical simulation presented in Fig. 4 show that in fact both the St(max) and St(0) adaptive systems demonstrate efficient phase-distortion compensation over a range far beyond the vicinity of small-amplitude phase distortions. After ten iterations a Strehl ratio level better than 0.95 was achieved for phase-distortion amplitudes in the ranges $0 < \sigma_{\text{in}} \leqslant 1.7$ rad for St(0) and $0 < \sigma_{\text{in}} \leqslant 2.6$ rad for St(max) systems. The adaptive system with the optoelectronic Zernike filter has an advantage in convergence speed for large-amplitude phase-distortion compensation.

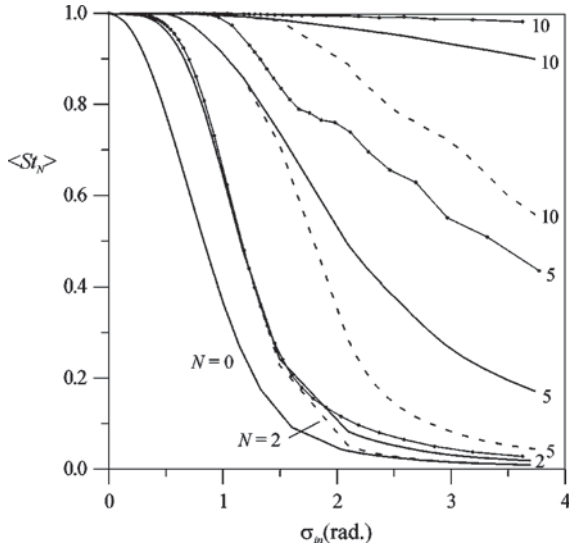

Fig. 4. Averaged Strehl ratio achieved after N iterations of the adaptation process versus input phase standard deviation for the following adaptive system configurations: St(0) system (dashed curves), St(max) (solid curves); $\text{St}_{\text{dif}}(\max)$ (solid curves with dots). Numbers near the curves correspond to the number of iterations N; the curve with $N = 0$ corresponds to $K = 0$ (no adaptation). Other parameters are the same as in Fig. 2.

B. Adaptive System with a Nonlinear Zernike Filter

The nonlinear Zernike filter introduced in Part I[1] can also be used as a wave-front sensor in a direct-control adaptive system. The structure of the adaptive controller (18) remains the same, except that $I_{\text{out}}(\mathbf{r})$ represents the output intensity of the nonlinear Zernike sensor. In the nonlinear Zernike filter the phase SLM placed in the sensor's focal plane introduces a phase shift θ dependent on the focal plane's intensity distribution $I_F(\mathbf{q})$, i.e., $\theta = \theta(I_F)$. In numerical simulations we considered a simple model for the phase SLM, with a phase shift proportional to the focal plane intensity: $\theta = \alpha I_F$, where α is a phase-modulation coefficient. Results of the numerical analysis for the corresponding adaptive system are presented in Fig. 5 for different phase-modulation coefficients α. The adaptive feedback system based on the nonlinear Zernike filter is capable of compensating phase distortions with an amplitude in the range of $\sigma_{\text{in}} \approx 1.2$ rad. Increasing α up to $\alpha \approx \pi/I_F^0$ leads to some extension of this range but causes performance degradation in the region $0.5 < \sigma_{\text{in}} \leqslant 1.2$ rad: The Strehl ratio is near 0.95 for $\alpha = \pi/I_F^0$ and near 0.98 for $\alpha = 0.5\pi/I_F^0$ (compare curves 3 and 4 of Fig. 5). This result suggests a control strategy with coefficients α that can be changed

during the adaptation process, dependent on the residual phase amplitude. In the region of large-amplitude phase distortions ($\sigma_{\text{in}} > 2.0$ rad) the value of α should be near π/I_F^0, or even larger; during the adaptation process it should be decreased to the value $\alpha = 0.5\pi/I_F^0$. This adaptive adjustment of the phase modulation coefficients has been realized in the experiments described below.

C. Adaptation in the Presence of Intensity Scintillations

Input wave intensity scintillations impose serious problems for conventional adaptive optics based on the phase reconstruction technique. They significantly limit the performance of adaptive optics for such important applications as laser communication, ground-to-ground long-range imaging, laser target designation, etc.[20,21] In this section we consider the results of a numerical analysis of direct-control adaptive systems with Zernike wave-front sensors in the presence of moderate and strong intensity scintillations. The input wave complex amplitude used in the calculations, $A_{\text{in}}(\mathbf{r}) = A_0(\mathbf{r})\exp[i\varphi(\mathbf{r})]$, had both random amplitude $A_0(\mathbf{r})$ and random phase $\varphi(\mathbf{r})$. To generate random input amplitudes (amplitude screens), realizations of a statistically homogeneous and isotropic random function $\zeta(\mathbf{r})$ with zero mean and a Gaussian model for the power spectrum were used. The spatial correlation radius of the random field $\zeta(\mathbf{r})$ is characterized by the parameter r_ζ normalized by the input aperture radius a. Input amplitudes are represented in the following two forms:

$$A_0(\mathbf{r}) = [1 + \alpha_{\text{am}}\zeta(\mathbf{r})]/\chi, \tag{19a}$$

$$A_0(\mathbf{r}) = |\alpha_{\text{am}}\zeta(\mathbf{r})|^2/\chi, \tag{19b}$$

where $\alpha_{\text{am}} = \omega/\max[\zeta(\mathbf{r})]$ and ω is a coefficient characterizing the depth of the amplitude modulation. The normalization coefficient χ in Eqs. (19) was used to preserve the same value of the aperture-averaged input field intensity for all random realizations: $\bar{I} = |\bar{A}_0|^2 = \text{constant}$. Input wave intensity modulation strength was characterized by the normalized standard deviation of the intensity fluctuation averaged over the aperture, σ_I, defined as $\sigma_I^2 = \int[I(\mathbf{r}) - \bar{I}]^2 d^2\mathbf{r}/\bar{I}^2$. Characteristic random patterns of the input-wave intensity modulation are shown in Fig. 6.

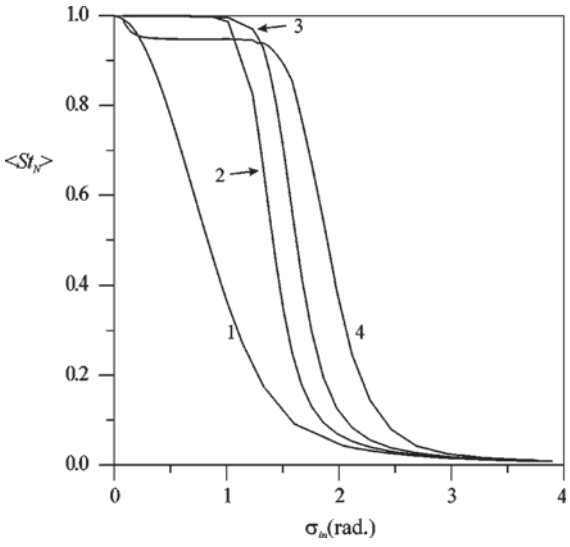

Fig. 5. Simulation results for an adaptive system with a nonlinear Zernike filter for different phase-modulation coefficients α: curve 1, $\alpha = 0$ (no adaptation); curve 2, $\alpha = 0.25\pi/I_F^0$; curve 3, $0.5\pi/I_F^0$; curve 4, $\alpha = 1.0\pi/I_F^0$. Other parameters are the same as in Fig. 2.

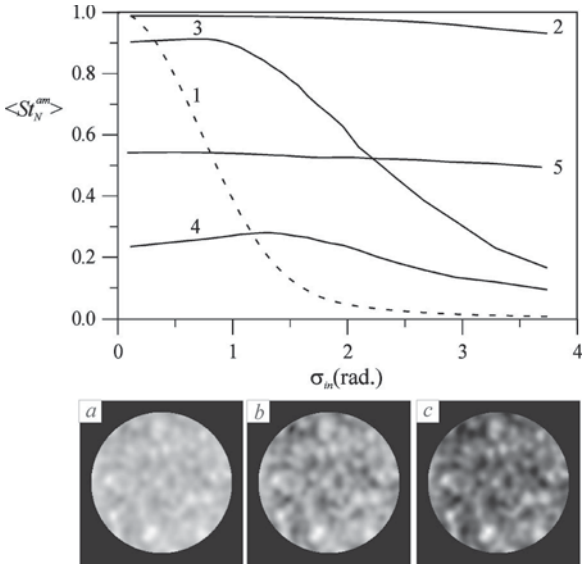

Fig. 6. Adaptive direct-control system with an optoelectronic Zernike wave-front sensor [St(max) configuration] in the presence of input field intensity scintillations. Averaged Strehl ratio achieved after 20 iterations of the adaptation process (18) versus input phase standard deviation for different intensity fluctuation levels characterized by the intensity-fluctuation standard deviation σ_I: curve 1, no adaptation; curve 2, $\sigma_I = 0.15$; curve 3, $\sigma_I = 0.35$; curve 4, $\sigma_I = 0.64$. Curve 5 corresponds to modified algorithm (18) with $\sigma_I = 0.64$ and $\epsilon = 1.25$. Snapshots of the input field intensity patterns for (a) $\sigma_I = 0.15$, (b) $\sigma_I = 0.35$, and (c) $\sigma_I = 0.64$. Other parameters are the same as in Fig. 2.

A fixed number of iterations N corresponding to control algorithm (18) were performed for each of 200 random input field realizations. System performance was evaluated by using the Strehl ratio $\text{St}_N^{\text{am}} = I_F(0)/I_F^0$ achieved at the end of adaptation (after N iterations), where I_F^0 is the intensity in the absence of phase aberrations. Note that I_F^0 corresponds to an input wave with random intensity modulation and uniform phase and hence is dependent on the random wave amplitude realization $A_0(\mathbf{r})$. For each Fried radius value r_0 and fixed intensity modulation correlation radius ($r_\zeta = 0.2a$), 200 values of the Strehl ratio St_N^{am} were obtained.

Averaged Strehl ratio $\langle \text{St}_N^{\text{am}} \rangle$ as a function of the input phase distortion standard deviation σ_{in} is shown in Fig. 6 for the adaptive system with an optoelectronic Zernike filter [St(max) system]. For relatively small-amplitude intensity modulation ($\sigma_I = 0.15$) the adaptive system was able to effectively suppress phase distortions in the phase-distortion range considered (see curve 2 in Fig. 6). When the intensity modulation level was increased, the phase-distortion compensation performance declined dramatically. The Strehl ratio achieved after 20 iterations was less than 0.9 for $\sigma_I = 0.34$ (curve 3) and only near 0.3 for $\sigma_I = 0.64$ (curve 4). Degradation in system perfor-

mance occurred even in the vicinity of small-amplitude input field phase distortions. In fact, in this region adaptation resulted in such undesirable effects as an increase in phase aberrations: Compare system performance with no adaptation (curve 1) and with adaptive wave-front control in the presence of strong intensity modulation (curve 4). This negative effect can be explained by the influence of the additional terms in the feedback controller [Eq. (17)] dependent on input field intensity modulation, as discussed in Section 3. Because of these terms, control algorithm (17) does not represent pure gradient-flow dynamics. This results in the appearance of a parasitic phase modulation that is proportional to the input field intensity modulation. In accordance with Eq. (17), we can decrease the influence of the input wave intensity modulation by subtracting from the wave-front sensor intensity distribution the term proportional to the input intensity $I_0(\mathbf{r})$. This would require an additional optical sensor capable of registering wave-front sensor input intensity. The modified feedback controller reads

$$u^{(n+1)}(\mathbf{r}) = u^{(n)}(\mathbf{r}) + d\nabla^2 u^{(n)}(\mathbf{r}) - K[I_{\text{out}}^{(n)}(\mathbf{r}) - \epsilon I_0(\mathbf{r})] - \mu[\bar{u}^{(n)} - u_0], \tag{20}$$

where $I_{\text{out}}^{(n)}(\mathbf{r})$ is the output intensity of either the conventional or the optoelectronic Zernike filter at the nth iteration and ϵ is a coefficient. Results of calculations with the modified feedback controller (20) are shown in Fig. 6 (curve 5). Subtraction of the input field intensity resulted in a significant increase in adaptive correction performance.

As discussed in Section 3, the feedback controller with a differential Zernike filter provides gradient-flow optimization of the Strehl ratio even in the presence of the input field's intensity modulation. The results of the numerical simulations presented in Fig. 7 support this conclusion.

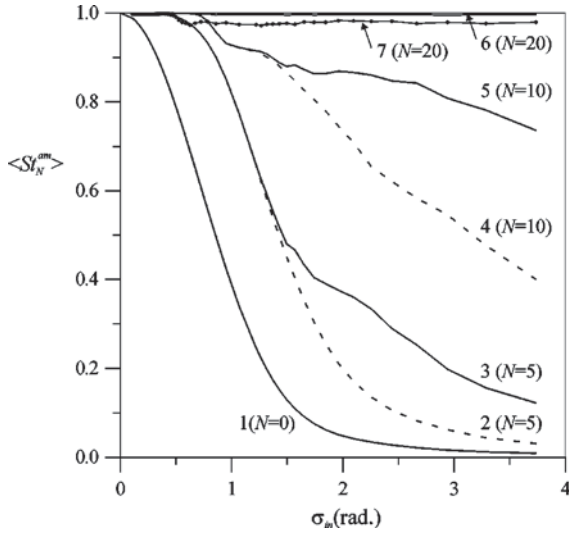

Fig. 7. Adaptive system with a differential Zernike wave-front sensor in the presence of input field intensity scintillations: St(max) configuration (solid curves) and St(0) configuration (dashed curves). Averaged Strehl ratio achieved after N iterations of the adaptation process versus input phase standard deviation for $K = 0.8$ and $\sigma_I = 0.35$ (curves 2–6) and $\sigma_I = 0.64$ (curve 7). Curve 1 corresponds to $K = 0$ (no adaptation). The number of iterations for each curve is shown parentheses.

Calculations were performed for an input field with intensity scintillations described by Eq. (19a) with $\sigma_I = 0.34$ and (19b) with $\sigma_I = 0.64$. The adaptive system with the differential Zernike wave-front sensor demonstrated efficient phase-distortion compensation over the entire examined region ($0 < \sigma_{\text{in}} < 4.0$ rad), independent of the input field intensity fluctuation level. For the $\text{St}_{\text{dif}}(\text{max})$ system configuration, approximately 20 iterations were required for Strehl ratios of $\text{St}_N^{\text{am}} \approx 0.99$ for $\sigma_I = 0.34$ (see curve 6 in Fig. 7) and $\text{St}_N^{\text{am}} \approx 0.975$ for $\sigma_I = 0.64$ (see curve 7). The convergence speed for the $\text{St}_{\text{dif}}(0)$ system was noticeably less in the region $\sigma_{\text{in}} > 1.5$ rad and was practically the same in the region of small-amplitude phase distortions (compare adaptation curves 2 and 3, and 4 and 5). The major effect of input field intensity scintillations on the performance of the adaptive system with the differential Zernike filter is that the adaptation convergence speed declined when the intensity scintillation level was increased (compare adaptation curves in Fig. 4 obtained for uniform intensity and those of Fig. 7). When the intensity modulation was $\sigma_I = 0.64$, approximately twice as many iterations were required for achieving the same Strehl ratio as in the case of uniform intensity.

This effect can be explained by using Eq. (7), which describes the wave-front control algorithm for a differential Zernike sensor. The presence of the intensity modulation in Eq. (7) leads to an effect similar to using a spatially modulated feedback gain coefficient of $K(\mathbf{r}) \approx KA_0(\mathbf{r})$. Thus, in the input field regions with low intensity levels, the feedback gain coefficient is small, resulting in a convergence rate decrease. Increasing the gain coefficient K may speed up the adaptation process, but only to a rather limited extent. In the region of input wave bright spots, the gain coefficient should be less than some threshold value K_{th}. For $K > K_{\text{th}}$ the discrete approximation of the feedback controller (18) is not stable, resulting in spatiotemporal instability of the entire adaptive system. A more efficient way to speed up the adaptation process is to use a spatially modulated gain coefficient that is higher in the "dark" regions and lower in the regions of the input wave "bright" spots. An analysis of the efficiency of this approach is beyond the scope of this paper.

5. ADAPTIVE SYSTEM WITH A NONLINEAR ZERNIKE SENSOR: EXPERIMENTAL RESULTS

The direct-control adaptive feedback system was investigated experimentally by using a nonlinear Zernike filter based on the LC light valve (LCLV) described in Part I.[1] A schematic diagram of the experimental setup is shown in Fig. 8. The laser beam from the He–Ne laser (12-mm diameter) entered the system and sequentially passed through two multielectrode LC spatial phase modulators HEX127 (SLM_1 and SLM_2) from Meadowlark Optics. The HEX127 LC phase modulators contain 127 independently controllable, hexagonal LC cells. SLM_1 was used

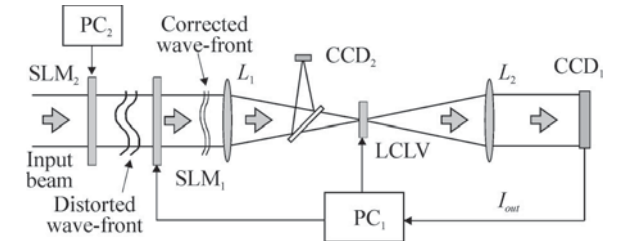

Fig. 8. Schematic of experimental setup for adaptive wave-front phase distortion compensation with a LCLV-based Zernike filter.

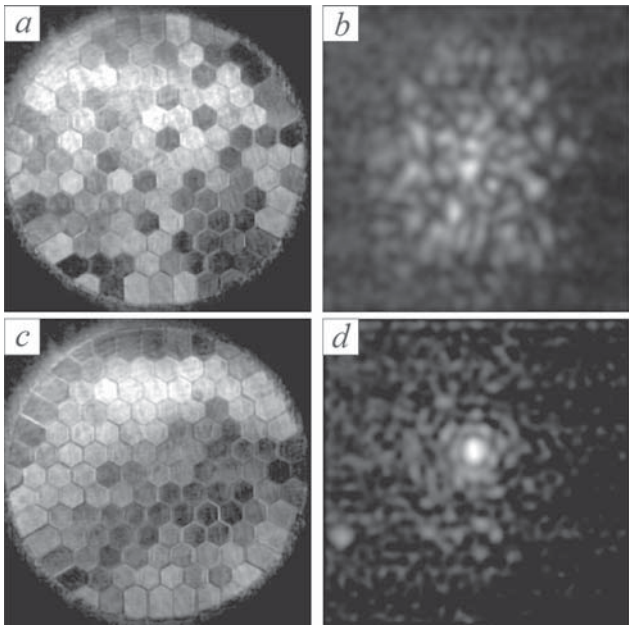

Fig. 9. Experimental results for an adaptive system with a nonlinear Zernike wave-front sensor: (a) interference pattern for the aberrated beam; (b) corresponding intensity distribution in the lens focal plane registered by the camera CCD_2 (Fig. 8); (c) and (d) are the same but for the corrected wave front.

to correct static random phase distortions introduced by the second phase modulator, SLM_2. This phase SLM was controlled with use of a computer (PC_2). The amplitude of the introduced phase distortions was in the range $[0, 3\pi$ rad].

The phase-distorted wave entered the nonlinear Zernike filter, which contained two identical lenses (L_1 and L_2) with 300-mm focal lengths and the optically addressed LCLV described in Part I.[1] Output intensity from the nonlinear Zernike filter was captured by a camera (CCD_1) and sent to a computer (PC_1), which implemented the feedback algorithm (18) with no diffusion term. The intensity distribution of the corrected beam in the focal plane of lens L_1 was registered by another camera (CCD_2). To improve the contrast of the nonlinear Zernike sensor output, the ac bias voltage V applied to the LCLV was controlled electronically, thus providing adaptive changing of the phase-modulation coefficient α during the adaptation process. The voltage amplitude V was dependent on the computed aperture-averaged variance of the Zernike filter output intensity distribution. This applied voltage amplitude V was decreased from 6 V at the beginning of adaptation to 2.4 V at the end.

Figure 9 shows experimental results of adaptive wave-front phase-distortion correction in the direct-control system with the nonlinear Zernike filter. Before adaptation, random voltages were applied to the phase modulator (SLM_2). For independent analysis of wave-front aberrations during the adaptation process we used a Mach–Zehnder interferometer (not shown in Fig. 8). An interference pattern corresponding to an initially phase-distorted wave is shown in Fig. 9a. The initial random phase modulation resulted in the random intensity-distribution pattern in the lens L_1 focal plane, as shown in Fig. 9b. Adaptation resulted in compensation of the introduced random phase distortion, except for wave-front tilts. The interference pattern of the wave front after 34 iterations of adaptive correction is shown in Fig. 9c, and the corresponding intensity distribution in the lens focal plane is shown in Fig. 9d. The amplitude astigmatism of $\sim$0.25 wavelength seen in Fig. 9c is related to wave-front aberration of the Mach–Zehnder interferometer reference wave. A factor-of-8 improvement in the Strehl ratio St(max) was obtained for the case shown in Fig. 9. Each iteration took $\sim$2 s, with most of the delay used to ensure that the phase-correcting SLM was fully updated between iterations. The Strehl ratio achieved was near 0.85, which is less than what was obtained in the simulations described above with the ideal noiseless nonlinear Zernike filter and high-resolution wave-front corrector.

The analysis and experiments considered a monochromatic light source. How important is this assumption, and what kinds of changes in system performance should be expected when a broadband light source is used instead? Increasing the input wave bandwidth Δ causes a degradation of Zernike wave-front sensor efficiency: The visibility of phase visualization by the wave-front sensor decreases, and at some point the bandwidth increase may result in a change of the sensor's output-intensity-contrast sign, leading to "wrong" (positive) feedback sign and to control system instability.

Indeed, the phase shift $\theta_0 = \pi/2$ introduced by the Zernike plate is optimal only for a specified wavelength λ_0. For a wavelength λ_1 ($\lambda_1 = \lambda_0 \pm \Delta/2$), the same phase-shifting Zernike plate gives the phase shift $\theta = (\pi/2)(\lambda_0/\lambda_1)$. The analysis shows that the adaptive direct-control system based on the Zernike wave-front sensor still works if the phase shift θ provides a sufficiently high-contrast wave-front sensor output and negative feedback. For a rough estimation, consider a phase-shift deviation of $\delta\theta$ from the optimal value $\theta_0 = \pi/2$ equaling $\delta\theta = \pm\pi/8$, a value acceptable from the viewpoint of control system stability. This gives a rough estimate of the light source bandwidth of $\Delta \approx 0.4\lambda_0$. It follows that the adaptive systems with Zernike wave-front sensors considered here may be used with a white light source.

6. CONCLUSION

The direct-control adaptive optics technique presented here offers an attractive alternative both to the conventional phase-conjugation adaptive system[22] and to adaptive optics based on model-free optimization techniques.[23] Unlike the conventional phase-conjugation approach, the

direct-control adaptive optics paradigm does not require wave-front reconstruction and can be used for high-resolution adaptive wave-front control. Similarly to model-free gradient-descent optimization techniques, the direct-control approach is based on gradient-descent optimization but considers gradient-flow optimization. This results in dramatic improvement in adaptation process convergence speed compared with that of model-free optimization adaptive optics. The key element of the direct-control adaptive optical system is the wave-front sensor, which is used not for wave-front reconstruction as in conventional adaptive optics but rather for measuring the gradient of the optimized cost function (in our case the gradient of the Strehl ratio). It is shown that wave-front sensors based on advanced phase-contrast techniques can provide information about the cost function gradient that can be used for synthesis of the gradient-flow feedback controller. The best adaptive system performance can be achieved with a differential Zernike filter, as the output of the filter is proportional to the Strehl ratio gradient. It is important that the adaptive system with the differential Zernike wave-front sensor be efficient for compensating phase distortions, even in the presence of strong intensity scintillations.

A practical implementation of the direct-control adaptive system requires both the development of advanced phase-contrast wave-front sensors as discussed in Part I,[1] and a VLSI parallel computational controller to interface the wave-front sensor and the wave-front shaping device.

APPENDIX A

Consider the cost functional (4):

$$J[u] = \left| \int A_0(\mathbf{r}) \exp\{i[u(\mathbf{r}) + \tilde{\varphi}(\mathbf{r})]\} \mathrm{d}^2\mathbf{r} \right|^2 - \beta_1 \left[u_0 - S^{-1} \int u(\mathbf{r}) \mathrm{d}^2\mathbf{r} \right]^2 - \beta_2 \int |\nabla u(\mathbf{r})|^2 \mathrm{d}^2\mathbf{r}. \tag{A1}$$

Represent Eq. (A1) in the form

$$J[u] = \bar{A}_0 \bar{A}_0^* - \beta_1 [\bar{u} - u_0]^2 - \beta_2 \int |\nabla u(\mathbf{r})|^2 \mathrm{d}^2\mathbf{r},$$

$$\bar{A}_0 = \int A_0(\mathbf{r}) \exp\{i[u(\mathbf{r}) + \tilde{\varphi}(\mathbf{r})]\} \mathrm{d}^2\mathbf{r}. \tag{A2}$$

Introduce a small perturbation in the controlling phase δu. Neglecting second- and higher-order terms with respect to δu, the perturbation of the cost functional δJ is

$$\begin{aligned} \delta J &= \bar{A}_0 \delta \bar{A}_0^* + \bar{A}_0^* \delta \bar{A}_0 - 2\beta_1 S^{-1} [\bar{u} - u_0] \times \int \delta u(\mathbf{r}) \mathrm{d}^2\mathbf{r} - 2\beta_2 \int \nabla u \nabla \delta u \, \mathrm{d}^2\mathbf{r} \\ &= |\bar{A}_0| [\exp(i\Delta) \delta \bar{A}_0^* + \exp(-i\Delta) \delta \bar{A}_0] - 2\beta_1 S^{-1} [\bar{u} - u_0] \int \delta u(\mathbf{r}) \mathrm{d}^2\mathbf{r} + 2\beta_2 \int (\nabla^2 u) \delta u \, \mathrm{d}^2\mathbf{r}. \end{aligned} \tag{A3}$$

Here $\bar{A}_0 = |\bar{A}_0| \exp(i\Delta)$. Represent $\delta \bar{A}_0$ and $\delta \bar{A}_0^*$ in the form

$$\delta \bar{A}_0 = i \int A_0 \exp\{i[u + \tilde{\varphi}]\} \delta u \, \mathrm{d}^2\mathbf{r},$$

$$\delta \bar{A}_0^* = -i \int A_0 \exp\{-i[u + \tilde{\varphi}]\} \delta u \, \mathrm{d}^2\mathbf{r}.$$

Substituting $\delta \bar{A}_0$ and $\delta \bar{A}_0^*$ into Eq. (A3) gives

$$\begin{aligned} \delta J = &-2|\bar{A}_0| \int A_0(\mathbf{r}) \sin[u(\mathbf{r}) + \tilde{\varphi}(\mathbf{r}) - \Delta] \delta u(\mathbf{r}) \mathrm{d}^2\mathbf{r} \\ &- 2\beta_1 S^{-1} [\bar{u} - u_0] \int \delta u(\mathbf{r}) \mathrm{d}^2\mathbf{r} \\ &+ 2\beta \int \nabla^2 u(r) \delta u(\mathbf{r}) \mathrm{d}^2\mathbf{r}. \end{aligned} \tag{A4}$$

From Eq. (A4) and the definition of the gradient as the linear part of the functional variation with respect to variation of the control function, we obtain

$$\begin{aligned} J' = &-2|\bar{A}_0| A_0(\mathbf{r}) \sin[u(\mathbf{r}) + \tilde{\varphi}(\mathbf{r}) - \Delta] \\ &- 2\beta_1 S^{-1} (\bar{u} - u_0) + 2\beta_2 \nabla^2 u(\mathbf{r}). \end{aligned} \tag{A5}$$

ACKNOWLEDGMENTS

We thank J. C. Ricklin for technical and editorial comments. This research was performed at the U.S. Army Research Laboratory's Intelligent Optics Lab in Adelphi, Maryland. It was supported in part by grants from the U.S. Army Research Office under Multi-University Research Inititative 97 program grant DAAG55-97-1-0114 to the Center for Dynamics and Control of Smart Structures (through Harvard University).

M. A. Vorontsov can be reached at U.S. Army Research Laboratory, AMSRL-CI-C, 2800 Powder Mill Road, Adelphi, Maryland 20783; mvorontsov@arl.army.mil; phone, 301-394-0214; fax, 301-394-0225.

REFERENCES

1. M. A. Vorontsov, E. W. Justh, and Leonid A. Beresnev, "Adaptive Optics with advanced phase-contrast techniques: 1. High-resolution wave-front sensing," J. Opt. Soc. Am. A **18**, 1289–1299 (2001).
2. V. P. Sivokon and M. A. Vorontsov, "High-resolution adaptive phase distortion suppression based solely on intensity information," J. Opt. Soc. Am. A **15**, 234–247 (1998).
3. M. A. Vorontsov, "High-resolution adaptive phase distortion compensation using a diffractive-feedback system: experimental results," J. Opt. Soc. Am. A **16**, 2567–2573 (1999).
4. R. A. Muller and A. Buffington, "Real-time correction of atmospherically degraded telescope images through image sharpening," J. Opt. Soc. Am. **64**, 1200–1210 (1974).
5. T. R. O'Meara, "The multi-dither principle in adaptive optics," J. Opt. Soc. Am. **67**, 306–315 (1977).
6. M. A. Vorontsov and V. I. Shmalhauzen, *Principles of Adaptive Optics* (Nauka, Moscow, 1985).
7. J. C. Spall, "A stochastic approximation technique for generating maximum likelihood parameter estimates," in *Proceedings of the American Control Conference* (Institute of Electrical and Electronics Engineers, New York, 1987), pp. 1161-1167.

8. G. Cauwenberghs, "A fast stochastic error-descent algorithm for supervised learning and optimization," in *Advances in Neural Information Processing Systems*, S. J. Hanson, J. D. Cowan, and C. L. Giles, eds. (Morgan Kaufman, San Mateo, Calif., Vol. 5, pp. 244–251, 1993).
9. M. A. Vorontsov, G. W. Carhart, and J. C. Ricklin, "Adaptive phase-distortion correction based on parallel gradient-descent optimization," Opt. Lett. **22**, 907–909 (1997).
10. M. A. Vorontsov and V. P. Sivokon, "Stochastic parallel gradient descent technique for high-resolution wavefront phase distortion correction," J. Opt. Soc. Am. A **15**, 2745–2758 (1998).
11. B. M. ter Haar Romey, ed., *Geometry-Driven Diffusion in Computer Vision* (Kluwer-Academic, Dordrecht, The Netherlands, 1994).
12. IEEE Trans. Image Process. Special issue on partial differential equations and geometry-driven diffusion in image processing and analysis, IEEE Trans. Image Process. **7**(3), (1998).
13. M. A. Vorontsov, "Parallel image processing based on an evolution equation with anisotropic gain: integrated optoelectronic architectures," J. Opt. Soc. Am. A **16**, 1623–1637 (1999).
14. G. Cauwenberghs and M. A. Bayoumi, eds., *Learning on Silicon* (Kluwer Academic, Dordrecht, The Netherlands, 1999).
15. A. G. Andreou and K. A. Boahen, "Translinear circuits in subthreshold MOS," Analog Integr. Circuits Signal Process. **9**, 141–166 (1996).
16. L. C. Andrews, "An analytic model for the refractive index power spectrum and its application to optical scintillations in the atmosphere," J. Mod. Opt. **39**, 1849–1853 (1992).
17. A. S. Michailov, and A. Yu. Loscutov, *Foundation of Synergetics* (Springer-Verlag, Berlin, 1991).
18. D. L. Fried, "Branch point problem in adaptive optics," J. Opt. Soc. Am. A **15**, 2759–2768 (1998).
19. D. L. Fried, "Statistics of a geometric representation of wavefront distortion," J. Opt. Soc. Am. **55**, 1427–1435 (1965).
20. C. A. Primmerman, T. R. Price, R. A. Humphreys, B. G. Zollars, H. T. Barclay, and J. Hermann, "Atmospheric-compensation experiments in strong-scintillation conditions," Appl. Opt. **34**, 2081–2088 (1995).
21. B. M. Levine, A. Wirth, H. DaSilva, F. M. Landers, S. Kahalas, T. L. Bruno, P. R. Barbier, D. W. Rush, P. Polak-Dingels, G. L. Burdge, and D. P. Looze, "Active compensation for horizontal line-of-sight turbulence over near-ground paths," in *Broadband Networking Technologies*, S. Civanlar and I. Widjaja, eds., Proc. SPIE **3233**, 221–232 (1998).
22. F. Roddier, ed., *Adaptive Optics in Astronomy* (Cambridge U. Press, Cambridge, UK, 1999), pp. 91–130.
23. M. A. Vorontsov, G. W. Carhart, M. Cohen, and G. Cauwenberghs, "Adaptive optics based on analog parallel stochastic optimization: analysis and experimental demonstration," J. Opt. Soc. Am. A **17**, 1440–1453 (2000).